HHS Public Access

Author manuscript

IEEE J Electromagn RF Microw Med Biol. Author manuscript; available in PMC 2022 September 01.

Published in final edited form as:

IEEE J Electromagn RF Microw Med Biol. 2022 September ; 6(3): 355–363. doi:10.1109/jerm.2021.3137962.

Development of a Coherent Model for Radiometric Core Body Temperature Sensing

Katrina Tisdale [Member, IEEE],

Alexandra Bringer [Member, IEEE],

Asimina Kiourti [Senior Member, IEEE]

Ohio State University ElectroScience Laboratory, Columbus, OH 43212 USA.

Abstract

This paper examines the utility of a wideband, physics-based model to determine human core body or brain temperature via microwave radiometry. Pennes's bioheat equation is applied to a six-layer human head model to generate the expected layered temperature profile during the development of a fever. The resulting temperature profile is fed into the forward electromagnetic (EM) model to determine the emitted brightness temperature at various points in time. To accurately retrieve physical temperature via radiometry, the utilized model must incorporate population variation statistics and cover a wide frequency band. The effect of human population variation on emitted brightness temperature is studied by varying the relevant thermal and EM parameters, and brightness temperature emissions are simulated from 0.1 MHz to 10 GHz. A Monte Carlo simulation combined with literature-derived statistical distributions for the thermal and EM parameters is performed to analyze population-level variation in resulting brightness temperature. Variation in thermal parameters affects the offset of the resulting brightness temperature signature, while EM parameter variation shifts the key maxima and minima of the signature. The layering of high and low permittivity layers creates these key maxima and minima via wave interference. This study is one of the first to apply a coherent model to and the first to examine the effect of population-representative variable distributions on radiometry for core temperature measurement. These results better inform the development of an on-body radiometer useful for core body temperature measurement across the human population.

Index Terms—

Biohea; coherent model; core body temperature; microwave thermometry; on-body radiometry

I. Introduction

CORE body temperature monitoring within at least 0.5°C [1] is critical for applications as diverse as precision cooling of the brain to minimize damage after traumatic brain injury [2] to monitoring athletes for hyperthermia [3]. Unfortunately, current standards of

Corresponding author: Katrina Tisdale, tisdale.58@osu.edu.

measuring core body temperature are either highly invasive or inaccurate, and therefore such measurements are often not treated with the same importance as other vital signs. Zero-heat-flux thermometers have been proposed as a noninvasive and accurate solution [4], [5] for the operating room. However, they are unable to detect intense body temperature changes and cannot measure a patient in deep hypothermia, both of which are experienced during many cardiac surgeries, among others [6]–[8].

Microwave radiometry is a noninvasive method that has the potential to overcome these limitations. This method uses an antenna to collect the microwave energy naturally emitted by the body and correlates the recorded brightness temperature with an absolute temperature via modeling. Microwave radiometry has been pursued in the past [2], [3], [9]–[15], though has yet to prove feasible in real-world scenarios primarily due to two main shortcomings:

a. Narrowband models and measurements [3], [16]–[19]. Narrow bandwidth radiometry limits the amount of data gathered from a sample because different frequencies penetrate different distances through the lossy tissues (i.e., longer wavelengths penetrate further through biological tissues and shorter wavelengths attenuate more quickly, meaning lower frequencies originate from deeper depths and vice versa). Most groups use a single frequency band with few using multiple frequencies (e.g., five frequencies from 1–4 GHz [17]). Limiting the number of frequencies in turn limits the information within a given radiometry measurement. Furthermore, many groups rely on modeling the antenna on the layered tissue profile via full-wave simulation software (e.g., Computer Simulation Technology (CST) Studio Suite [20]) to determine the emissions received from each layer [2], [3], [9], [10], [21]. To make up for the limited number of frequencies, skin surface temperature is then measured to back-calculate the temperature of the underlying layers. This method limits their modeling to their specific antenna and limits the accuracy to that of the skin surface temperature measurement, which is susceptible to many factors including ambient temperature [22].

b. Use of a single fully characterized phantom. Models and presented measurements are typically performed on fully characterized phantoms, accounting for only a single set of thermal and electromagnetic (EM) parameters and ignoring human variability. For example, [21] optimizes their antenna for their specific phantom's properties and measures the phantom's physical temperature throughout a heating and cooling experiment to within less than 0.4°C error. However, as per [9], [23]–[26], human tissues exhibit variations in their thermal and EM properties. As such, in [21] during measurements on a human baby undergoing surgery with properties different from those of the test phantom, the radiometer-measured temperature deviated from the medical-grade thermometers by anywhere from 1°C to 4.5°C throughout the surgery.

To this end, we present a wideband model for tissue radiometry. Specifically, we adapt a physics-based model used to measure the thermal emission of layered ice sheets in Greenland [27] to the layered configuration of human head tissues. We use a coherent model because it ignores volume scattering effects, which is justified by assuming homogenous

tissue layers and by the fact that wavelengths are much greater than the size of the scattering objects in each layer. Additionally, the coherent model is considered an exact model, rather than an approximation [28]. To eliminate the need for the accuracy-limiting skin surface measurement employed by the groups listed in shortcoming (a), we use the bioheat transfer model to obtain physical temperature for the coherent model calculation.

We analyze the feasibility of the coherent model for relating brightness and physical temperature of humans with one of the only compilations of population-representative distributions for the thermal and EM parameters necessary for on-body radiometry. These distributions, which we generate via literature review, allow us to assess the utility of the thermal-coherent model in real-life situations where the exact values of the thermal and EM parameters are unknown, as opposed to relying on a single mean profile to capture this population variation as did the groups listed in shortcoming (b). Overall, the model presented in this paper is a step towards developing a general on-body radiometer for core temperature measurement of all patients.

II. Methods and Procedures

A. Bioheat Model

The most commonly used model for determining bioheat transfer is Penne's bioheat equation [29]. This experimentally verified model remains the most widely implemented due to its "simplicity and acceptable accuracy" [16], [30]. The model for each tissue layer is represented as such:

$$k\nabla^2 T + \rho_b c_b \omega (T_a - T) + Q_m = \rho c \frac{\delta T}{\delta t} \quad (1)$$

where k is the given tissue's thermal conductivity, T is the layer temperature with the subscript a denoting the arterial or blood temperature, ρ is density, c is specific heat, ω is perfusion or blood flow rate, Q_m is basal or resting metabolic rate, and the subscript b denotes that the variable represents the given property of blood.

Pennes' bioheat equation is implemented in Dassault Systemes' CST Studio Suite [20]. The thermal parameters are specified for each "material" or tissue type, except for the tissue temperature, T, which is the quantity to be solved. The product of blood density, blood specific heat, and tissue perfusion are represented as a single parameter, B, called blood flow coefficient.

Since core temperature is defined via the blood in the hypothalamus and the brain is the key metabolic organ [31], noninvasively monitoring from the head surface is the ideal choice. On the head, a flat skin surface with minimal hair coverage is ideal for conforming to the typically flat bottom surface of antennas to eliminate EM-signal-degrading air gaps (assuming the antenna is matched to the tissue). These criteria indicate the forehead is the optimal monitoring location. The basic layered anatomy of the forehead from the surface to the core is shown in Fig. 1 and consists of skin, subcutaneous fat, muscle, skull, cerebrospinal fluid (CSF), and brain or core [32]. Thus, we use these six layers in our model.

1) Thermal Variable Distributions: To generate the population-representative thermal parameter distributions in Table I, a review of the literature relating to the measurement of the specific heat (c), thermal conductivity (k), basal metabolic rate (Q_m), blood flow coefficient (B), density (ρ), and tissue layer thickness (h) for the six tissues of our head model is performed. Though these measurements are not found in abundance in the literature, especially measured at the forehead, nine sources for each of the thermal-specific variables [16], [20], [33]–[39] and nine sources for the tissue layer thicknesses (which is also a direct input to the coherent model) are chosen [37], [40]–[47]. The sources selected for tissue layer thicknesses are measurement sets for the head and represent papers published by groups from different countries and therefore measurements of various populations. The thermal-specific variable papers are compilation papers, which review the literature. From this information, we generate normal distributions for the parameters.

2) Thermal Model Implementation: To simulate measuring a change in core temperature over time for the following studies on brightness temperature, we choose to model the initial development of a continuous fever from a core temperature of 37°C to 39°C, as described in [48]. We increase the temperature of the entire brain layer from the normothermic steady state and approach (but do not reach) the hyperthermic steady state over the course of 30 min and examine the change in the outer layers. Thus, we do not vary the thermal parameters of the brain in this study. This method simulates measuring the volume-averaged brain/core temperature, rather than localized brain temperature.

Additionally, as this study is designed to assess the effect of human variation on measured brightness temperature, the ambient air temperature is held constant at 25°C (the effect of ambient temperature can be explored in a future study). The skin surface boundary interacts with air via convective flow, and the remaining boundaries are adiabatic.

B. Coherent Model

The coherent model is based on the fluctuation-dissipation theorem, which relates the thermal vibrations of charges (molecules – electric dipoles, induced electric dipoles, etc. – all of which vibrate when physical temperature is above 0 K) in a medium to the current density in that medium. The EM field radiated due to these thermal vibrations is calculated using the dyadic Green's function. Maxwell's equations describe how the generated field propagates through the medium. For a medium with n layers, (2), shown at the bottom of this page, describes the resulting brightness temperature observed from an incidence angle of 0.

Here, T_l is the temperature of layer l (in general the subscript l denotes that variable is for the layer l); T_t is the temperature of the bottom layer (in general the subscript t denotes that variable is for the layer t); A_l, B_l are the field amplitude coefficients (which are solved using a recursive relation for the propagation matrix); d_l is the distance from the surface of the structure to layer l; and the rest of the variables are used as commonly found in EM (notably, T' is the transmission coefficient from the last to second to last layer). For coherent model layers, we subdivide each tissue layer for brightness temperature resolution (Fig. 1).

As this study is to demonstrate the feasibility of using the coherent model for tissue radiometry, we are exploring the use of this model with a planar layered tissue structure and examining the effects of population variation by varying tissue layer thickness, permittivity, and thermal properties. While anatomical differences in addition to layer thickness (e.g., head curvature) can affect wave propagation, we save the study of anatomical head models for future work, for which the current study serves as a foundation [26].

The coherent model assumes the sensed object is in the far field of the receiver. Thus, the envisioned system uses a high dielectric matching medium between the skin surface and the receiver to put the skin surface in the far field, as defined by the lowest operating frequency, while maximizing the received signal. For example, if the dielectric medium is designed to replicate the EM properties of skin as reported in [49], using the standard definition of the far field (namely, twice the square of the longest antenna dimension divided by the wavelength in the medium) and assuming the longest antenna dimension is approximately half of the longest operating wavelength (lowest frequency) in the medium, if the lowest operating frequency is 100 MHz, the medium should be at least 17 cm tall. For a 1 GHz low frequency cutoff, the medium should be at least 2.3 cm tall. While a 17 cm high medium might not be feasibly implemented in a real-world scenario, we include 100 MHz in the analysis to better understand the brightness temperature versus frequency spectrum produced by the human head.

1) EM Variable Distributions: To generate the population-representative EM variable distributions, that is real and imaginary permittivity, we first turn to the most widely used source for such information: [49], a database which is derived from the 4-pole Cole-Cole model in [50] determined via measurements across various human and animal cadavers and living humans [51], [52]. We use these profiles for our selected tissues as our mean. Many papers quote variation in permittivity as being ±20% [26], [53], which originates from [54] in which the

$$T_B = k\sum_{l=1}^{n}\frac{\varepsilon''_l T_l}{2\varepsilon_o}\left\{\frac{|A_l|^2}{k''_l}\left(e^{2k''_l d_l}-e^{2k''_l d_l-1}\right)-\frac{|B_l|^2}{k''_l}\left(e^{-2k''_l d_l}-e^{-2k''_l d_l-1}\right)\right.$$
$$\left.+\frac{iA_lB_l^*}{k'_l}\left(e^{-i2k'_l d_l}-e^{-i2k'_l d_l-1}\right)-\frac{iA_lB_l^*}{k'_l}\left(e^{i2k'_l d_l}-e^{-i2k'_l d_l-1}\right)\right\}+\frac{k\varepsilon''_l T_t}{2\varepsilon_o k''_t} \quad (2)$$
$$\left|\mathrm{T}\right|^2 e^{-2k''_t d_n}$$

worst-case specific absorption rate (SAR) scenario for children with cell phones is evaluated. This range is based on changes in total body water content with age via rat and pig permittivity studies [54]. However, in the absence of sufficient data on humans, real and imaginary permittivity variation measurements performed in animals [23]–[25] indicate a standard deviation of 10% is a likely worst case scenario. The real and imaginary permittivity vary separately (e.g., real permittivity is 105% and imaginary permittivity is 97% of the mean). Thus, we use a standard deviation of 10%.

2) Thermal and EM Parameter Effect on Brightness Temperature: To compare the effects of each of the thermal and EM parameters on brightness temperature, we use a common percentage by which to change each parameter. To ensure this common percentage holds a physical significance, the approximate average of the percentage of one standard deviation from the mean of all the thermal parameters, namely ±20%, is used. This common percentage provides a means by which the magnitude of the effect on physical and brightness temperature of each individual thermal and EM parameter can be compared. While the resulting change in physical and brightness temperature occurring due to a 0% to 20% parameter variation is not linear for the parameters, a 0% to 20% change in a given parameter results in a greater difference in either temperature than a 0% to 19% change.

Previous radiometry systems are limited by the use of narrowband antennas due to the challenge of designing a wideband antenna able to radiate into the human body, and therefore, their measurements are narrowband as well [3], [10], [18], [21]. Our group has pioneered the design of antennas for the human body with bandwidth and gain much greater than what is published in the literature [55]. Thus, we can realistically explore wider frequency ranges in our modeling. In this study, the coherent model is run from 0.1 to 10 GHz to assess brightness temperature across a wide frequency band and to find potential characteristics of the brightness temperature from the six-layer profile that can assist with future attempts at physical temperature retrieval.

To this end, we calculate the brightness temperature received at normal incidence, as in (2), for each scenario. Future studies will explore the optimal frequency band for a core body temperature radiometer. An antenna can then be designed to cover that bandwidth, and the coherent model would then be integrated over the beamwidth of the specified antenna, accounting for the vertically and horizontally polarized brightness temperature contributions as described in [28].

To assess the utility of the coherent model for use with the human population, the thermal-coherent model combination is run for 1000 iterations with all of the thermal and EM parameters varied via their population-representative distributions.

III. Results

A. Thermal Parameter Effect on Physical Temperature

To study the individual effect of each thermal parameter on the overall temperature profile of the tissues, each thermal parameter is individually changed to ±20% of its respective mean in each individual layer with the rest of the parameters held at their respective mean (e.g., the thermal conductivity is +20% of the mean in skin, while all other parameters, including thermal conductivities in the other layers, are set at their mean values). The brain temperature is increased from normothermic to hyperthermic to simulate fever development. At each measurement over the course of fever development, the average temperature of each layer of the resulting thermal profile is compared to the same layer of the thermal profile generated when all parameters are at their mean values. Table II lists the largest temperature difference for all layer comparisons (Max Δ°C) and the layer in which that difference occurs

(Layer), since the largest temperature difference does not necessarily occur in the layer in which the parameter is changed.

Thermal conductivity, k, and tissue layer thickness, h, affect both the steady state and transient profile as per (1). Both parameters have the largest effect on the thermal profile, shifting the temperature profile by at least 0.1°C for almost all iterations. Varying the skin blood flow coefficient, B, results in a comparably large change. For each parameter, any parameter change in a given layer affects the temperature of both that layer and the surrounding layers. This temperature change decreases further from the layer in which the parameter is varied. Based on these results, the effect of thermal conductivity and layer thickness, followed by skin perfusion, are key to examining population differences.

B. Thermal Parameter Effect on Brightness Temperature

The brightness temperature resulting from the ±20% thermal profiles of Section III-A is then calculated via (2). When analyzing the effect of the thermal parameters, each parameter, except for tissue layer thickness, only contributes to layer temperature, T_l (or T_t in the case of the brain), so any change in T_l scales (2). Tissue layer thickness, h, in addition to affecting the temperature profile (T_l), separately affects (2) via d. As such, tissue layer thickness is also considered an EM variable and is discussed in Section III-C.

Each of the thermal parameters, except for tissue layer thickness, produces a similar pattern of change in the brightness temperature as in the physical temperature. Fig. 2(a) shows the difference between the brightness temperature when all parameters are at their mean values and when the CSF thermal conductivity is varied by ±20% at 0, 10, and 30 min into the development of the hyperthermic core temperature. Fig. 2(b) shows the same for muscle specific heat. Since thermal conductivity affects the steady state and transient thermal profile, occurring at 0 min and 10 min, respectively, thermal conductivity likewise affects the brightness temperature both when the physical temperature is at steady state and is transient. Specific heat, however, only affects the transient physical temperature profile, and therefore varying the specific heat has no effect on brightness temperature when the physical temperature is unchanging (i.e., at 0 min). Varying density produces a very similar effect to varying specific heat. As per (1), metabolic rate produces a constant offset and results in a change to the steady state and transient profiles. Blood perfusion likewise changes both the steady state and transient profiles, with the effect depending on the difference between the blood and layer temperatures.

C. EM Parameter Effect on Brightness Temperature

The EM parameters (real and imaginary permittivity and layer thickness), unlike the thermal parameters, do not affect the temperature of the tissue but rather affect wave propagation through the layered tissue profile. As such, if the EM parameters are constant over time (i.e., they do not change as the fever progresses from normothermic to hyperthermic over 30 min, as is assumed in this study), only T_l and T_t vary with time in (2). Thus, the following evaluations of the effect of the EM parameters are done for the normothermic steady state (0 min) as any changes over time are caused by the changing temperature profile and not the EM parameters.

The solid green trace in Fig. 3(a) and (b) is the frequency-dependent brightness temperature evaluated when all thermal and EM parameters are at their mean values. Two distinct maxima exist and are due to the large difference in permittivity between the layers. The differences turn the skin, fat, muscle, and bone layers into cavity-like structures. These large differences in permittivity between adjacent layers cause a large reflection coefficient, creating more wave interference. The coherent model relies on wave propagation to determine the brightness temperature received at the surface; thus, the interference within the cavity-like layers causes the maxima and minima in the brightness temperature. Changing the EM parameters of one of these cavity-like layers produces a greater change in the resulting brightness temperature profile than one of the non-cavity-like layers.

For example, as per Fig. 3(a) and (b), the difference in brightness temperature at a given frequency and the frequencies at which maxima occur when CSF thickness is varied by ±20% compared to when all parameters are at their mean values is smaller than when skin thickness is varied. CSF and brain tissue have a similar permittivity, whereas skin has a high permittivity but is surrounded by air and fat, which have low permittivity. The difference in brightness temperature profiles caused by varying the CSF thickness is smaller compared to that of skin as a result, especially at the higher frequencies which do not travel as far through tissues as the lower frequencies (and therefore are less likely to reach a receiver at the surface if originating from the CSF).

A change in brightness temperature versus frequency can be represented as either a change in brightness temperature at a given frequency (e.g., a 0.5 K increase at 2.1 GHz) or as a change in the frequencies at which the two maxima occur. Fig. 4 displays the frequencies at which the high and low frequency maxima occur when each thermal and EM parameter is individually varied in each individual layer by ±20% (i.e., all other parameters are at their mean value, including the parameter of interest in the other five layers) compared to when all parameters are at their mean value (represented by the black dot).

Tissue layer thickness has the largest effect of the EM parameters on brightness temperature. As per Fig. 4, decreasing the tissue layer thickness shifts the peak brightness temperature frequency higher and vice versa for increasing tissue layer thickness. Varying real permittivity causes the next largest effect in terms of maxima frequency. For all layers except CSF, a decrease in real permittivity causes the maxima to shift to a higher frequency and vice versa for an increase. Minimal frequency shifting of the maxima is observed when imaginary permittivity is varied.

In general, a decrease in real permittivity causes an increase in the high frequency maximum, while the same pattern exists for the low frequency maximum for all layers except CSF. For imaginary permittivity, at the low frequency maximum, variation in CSF and muscle have the greatest effect because they are more lossy tissues and are located deeper in the tissue block. At the high frequency maximum, only muscle, a decrease in CSF, and an increase in skin imaginary permittivity affect the brightness temperature peak. The effect is caused by a combination of layer depth and mean permittivity (i.e., shallower layers with higher loss or the decrease of loss of deeper layers with high loss have a greater effect on the higher frequencies).

From this analysis, only a change in EM parameters can change the frequency where a maximum occurs. As per Figs. 2 and 4, changing the thermal parameters (except for layer thickness), only shifts the level of the brightness temperature at a given frequency, indicating the physical temperature profile itself is different, but does not change the frequency at which a maximum occurs. In general, if the EM parameters do not change over time, then the locations of the maxima will not change for a given simulation. Thus, a shift in maxima location can indicate a change in the EM parameters, while a change in brightness temperature at the maxima can indicate a change in physical temperature.

D. Population-Level Variation

To assess the error in brightness temperature from assuming a single profile based on the mean values of the thermal and EM parameters, a Monte Carlo simulation is set to determine the brightness temperature profiles that result from varying different combinations of each of the parameters. A total of 1000 iterations of the bioheat-coherent model combination are performed, with each of the parameters varying as per the normal distributions given in Table I. Though parameters may be related (e.g., how hydrated a person is can effect both blood flow coefficient and permittivity), finding these relations is outside of the scope of this paper, and so parameters vary independently according to their distributions.

Fig. 5 shows all the brightness temperatures for the 1000 iterations compared to the brightness temperature for all parameters set to their mean value (black dashed line) at 0 min, as well as the standard deviation in brightness temperature at a given frequency of the trials (the black bars). The smallest difference occurs at the lowest frequencies, which originate from deeper tissue layers, and is indicative of each profile having the same core temperature. This minimal difference indicates that despite the variation in the thermal and EM parameters of each of the layers, the same core temperature produces a similar brightness temperature profile at the deeper-penetrating lower frequencies.

The largest variation in brightness temperature spectra occurs around the high frequency maximum due to the shift in the frequency at which the high frequency maximum occurs. As explained in Section III-C, this shift in maxima frequencies is caused by EM parameter variation as would be exhibited when measuring two different people. Examining this shift in maxima frequencies, a standard deviation of 129.8 MHz occurs around the first maximum mean frequency of 1.09 GHz, whereas a standard deviation almost four times larger of 434.0 MHz occurs around the second maximum mean frequency of 3.58 GHz.

This variation in brightness temperature profiles holds implications for the physical temperature retrieval process. Many on-body radiometry papers assume a single mean profile to determine the weighting coefficient for how much power, or what portion of the total received brightness temperature, originates from each tissue layer [3], [10], [18], [21]. Many of these previous studies operate around 1 GHz, where the variation in brightness temperature becomes significant, as per Fig. 5. Even though all the profiles in Fig. 5 are generated with the same core temperature, if a single frequency is used and the mean profile is assumed, measuring anyone who exhibits one of the profiles other than the mean profile would incorrectly be measured as having a core temperature higher or lower than their actual core temperature. As per Section III-C, changes in the brightness temperature level

without a change in the maxima frequencies indicate a physical temperature change. Not acknowledging thermal and EM parameter variation across the population, as done in past works [3], [12], [17]–[19], [21], therefore, means that two people who have the same core temperature but different EM and thermal parameters would incorrectly receive different core temperature measurements. Additionally, if parameter variation is accounted for, one or even five frequencies spread from 1–4 GHz, as used in [3], [16]–[19], is not enough to indicate whether a change in maxima frequencies or a change in brightness temperature alone is the cause of the measured brightness temperature. Ignoring parameter variation limits the accuracy of retrieving a physical temperature profile for different humans.

Beyond core temperature retrieval, as per the large deviations in brightness temperature at higher frequencies, which originate from shallower depths than lower frequencies, retrieving a full temperature-vs.-depth profile requires sensing across a wider frequency band. Only receiving lower frequencies can lead to measuring incorrect physical temperatures in the shallower tissue layers given the small deviation in brightness temperature at lower frequencies for a given core temperature, as per Fig. 5.

IV. CONCLUSION

In this paper, we explore the use of a thermal and coherent model combination for radiometric core temperature sensing of a six-layer head model. Unlike previous attempts at tissue radiometry, we start with a wideband model to analyze trends in the brightness temperature generated by the natural thermal emissions of the human head. We do not rely on a single mean profile for the simulated phantom, but rather, with human population-based statistical distributions for the thermal and EM parameters, we show that such reliance can result in an error between the expected and resulting brightness temperature for a given core temperature or physical temperature profile. The minimal change at lower frequencies and larger change at higher frequencies indicates that a wideband model is necessary to indicate whether a change in brightness temperature is caused by a different set of thermal and EM parameters or by a different temperature profile, as well as to depict the full temperature profile of the six tissue layers. Based on the results of this study and the importance of accounting for the variation of the parameters, we will implement a retrieval algorithm to determine physical temperature from a given radiometric measurement while reducing the error seen in previous on-body radiometry attempts by accounting for population variation. We will also explore spherical and anatomical head models. Additionally, we will validate the use of this coherent model for on-body radiometry via experiments. Thus, this study progresses the field of on-body radiometry for a safer operating room and beyond by implementing the first wideband model that accounts for population variation.

Acknowledgment

The content is solely the responsibility of the authors and does not necessarily represent the official views of the National Institutes of Health.

This work was supported by the National Institute of Biomedical Imaging and Bioengineering of the National Institutes of Health under Grant R03EB030286. The work of Katrina Tisdale was supported by the National Defense Science and Engineering Graduate Fellowship.

Biographies

Katrina (Guido) Tisdale (Member, IEEE) received the B.S. degree in physics from the Stevens Institute of Technology in Hoboken, NJ, USA, in 2018. Since 2018, she has been working toward the doctorate degree in electrical engineering with The Ohio State University, Columbus, OH, USA.

She was an Intern with the National Institute of Standards and Technology, Boulder, CO, USA, in 2016, Pennsylvania State University Applied Research Laboratory, State College, PA, USA, in 2017, and Biosense Webster, Irvine, CA, USA, in 2021. She has authored several book chapters and conference and journal papers. Her research interests include medical sensing, implanted and wearable antennas for medical applications, phantom design, and bioelectromagnetics.

She is a Member of the Sigma Pi Sigma Physics Honors Society. She has won several fellowships and awards, including the National Defense Science and Engineering Graduate Fellowship 2019, Ohio State College of Engineering Fellowship 2018, Stevens Institute of Technology First in Class Lawrence C.F. Horle Memorial Award 2018, and First in Physics Alfred M. Mayer Prize 2018. In 2019, she was named a NIH BRAIN Initiative summer course scholar.

Alexandra Bringer (Member, IEEE) received the M.S. and Ph.D. degrees in physics from the Université du Sud-Toulon-Var, La Garde, France, in 2009 and 2012, respectively. She is currently with ElectroScience Laboratory, The Ohio State University, Columbus, OH, USA, as a Research Scientist. Her studies were focused on physical oceanography and remote sensing. In 2014, she joined ElectroScience Laboratory. Since then, she has been working on microwave radiometry for cryosphere applications and Radio Frequency Interference detection and mitigation. She is currently a Science Team Member for the Soil Moisture Active Passive Mission, Cyclone Global Navigation Satellite Systems and part of the soil moisture group for the NISAR Mission. Her research interests include Earth monitoring, microwave active and passive remote sensing for land, ocean, cryosphere and medical applications and signal processing. She is also the Chair of the IEEE Columbus Chapter Joint Section AP-S/MTT and a Member of the technical committee for Frequency Allocations in Remote Sensing.

Asimina Kiourti (Senior Member, IEEE) received the Diploma degree in electrical and computer engineering from the University of Patras, Patras, Greece, in 2008, the M.Sc. degree in technologies for broadband communications from University College London, London, U.K., in 2009, and the Ph.D. degree in electrical and computer engineering from the National Technical University of Athens, Athens, Greece, in 2013. She is currently an Assistant Professor of electrical and computer engineering with The Ohio State University and the ElectroScience Laboratory, Columbus, OH, USA. From 2013 to 2016, she was a Postdoctoral Researcher and then a Senior Research Associate with the ElectroScience Laboratory. During her career, she has authored more than 45 journal papers, 80 conference papers, nine book chapters, and eight patents. Her research interests include bio-electromagnetics, wearable and implantable antennas, sensors for body area applications, and functionalized e-textiles.

She was the recipient of several awards and scholarships, including the URSI Young Scientist Award for 2018, IEEE Engineering in Medicine and Biology Society Young Investigator Award for 2014, IEEE Microwave Theory and Techniques Society Graduate Fellowship for Medical Applications for 2012, and IEEE Antennas and Propagation Society Doctoral Research Award for 2011. She is currently an Associate Editor for the IEEE Transactions on Antennas and Propagation, IEEE Journal of Electromagnetics, RF and Microwaves in Medicine and Biology, and *Advanced Electromagnetics*.

References

[1]. Moran DS and Mendal L, “Core temperature measurement,” Sports Med., vol. 32, no. 14, pp. 879–885, 2002, doi: 10.2165/00007256-200232140-00001. [PubMed: 12427049]

[2]. Maruyma K et al. , “Feasibility of noninvasive measurement of deep brain temperature in newborn infants by multifrequency microwave radiometry,” IEEE Trans. Microw. Theory Techn, vol. 48, no. 11, pp. 2141–2147, Nov. 2000, doi: 10.1109/22.884206.

[3]. Momenroodaki P, Haines W, Fromandi M, and Popovic Z, “Noninvasive internal body temperature tracking with near-field microwave radiometry,” IEEE Trans. Microw. Theory Techn, vol. 66, no. 5, pp. 2535–2545, May 2018, doi: 10.1109/TMTT.2017.2776952.

[4]. “Tcore™ Temperature monitoring system safe, accurate, non-invasive,” Lubeck, Germany: Draeger, 2015, pp. 1–8. [Online]. Available: https://www.draeger.com/products/content/tcore-br-9069837-en.pdf

[5]. “Introducing the 3M spoton temperature monitoring system,” St. Paul, MN, USA: 3M, 2012, pp. 1–4. Accessed: May 6, 2019. [Online]. Available: www.spotontemperature.com

[6]. Sastre JA, Pascual MJ, and López T, “Evaluation of the novel non-invasive zero-heat-flux Tcore™ thermometer in cardiac surgical patients,” J. Clin. Monit. Comput, vol. 33, no. 1, pp. 165–172, Feb. 2019, doi: 10.1007/s10877-018-0143-2. [PubMed: 29667096]

[7]. Mäkinen MT et al. , “Novel zero-heat-flux deep body temperature measurement in lower extremity vascular and cardiac surgery,” J. Cardiothoracic Vasc. Anesth, vol. 30, no. 4, pp. 973–978, Aug. 2016, doi: 10.1053/j.jvca.2016.03.141.

[8]. Eshraghi Y et al. , “An evaluation of a zero-heat-flux cutaneous thermometer in cardiac surgical patients,” Anesth. Analg, vol. 119, no. 3, pp. 543–549, 2014, doi: 10.1213/ANE.0000000000000319. [PubMed: 25045862]

[9]. Hand JW et al. , “Monitoring of deep brain temperature in infants using multi-frequency microwave radiometry and thermal modelling,” Phys. Med. Biol, vol. 46, no. 7, pp. 1885–1903, 2001, doi: 10.1088/0031-9155/46/7/311. [PubMed: 11474932]

[10]. Bardati F, Brown VJ, Ross MP, and Tognolatti P, “Microwave radiometry for medical thermal imaging: Theory and experiment,” in Proc. IEEE MTT-S Int. Microw. Symp. Dig, 1992, vol. 3, pp. 1287–1290, doi: 10.1109/mwsym.1992.188237.

[11]. Cresson PY, Ricard C, Dubois L, Vaucher S, Lasri T, and Pribetich J, “Temperature measurement by microwave radiometry,” in Proc. Conf. Rec. - IEEE Instrum. Meas. Technol. Conf, 2008, pp. 1344–1349, doi: 10.1109/IMTC.2008.4547251.

[12]. Rodrigues DB et al. , “Numerical 3D modeling of heat transfer in human tissues for microwave radiometry monitoring of brown fat metabolism,” Energy-based Treat. Tissue Assessment VII, vol. 8584, Feb. 2013, Art. no. 85840S, doi: 10.1117/12.2004931.

[13]. Groumpas E, Koutsoupidou M, Karanasiou IS, Papageorgiou C, and Uzunoglu N, “Real-time passive brain monitoring system using near-field microwave radiometry,” IEEE Trans. Biomed. Eng, vol. 67, no. 1, pp. 158–165, Jan. 2020, doi: 10.1109/TBME.2019.2909994. [PubMed: 30969913]

[14]. Goryanin I et al. , “Passive microwave radiometry in biomedical studies,” Drug Discov. Today, vol. 25, no. 4, pp. 757–763, Apr. 2020, doi: 10.1016/J.DRUDIS.2020.01.016. [PubMed: 32004473]

[15]. Karanasiou IS and Uzunoglu NK, “Single-frequency and multiband microwave radiometry for feasible brain conductivity variation imaging during reactions to external stimuli,” Nucl. Instruments Methods Phys. Res. Sect. A Accel. Spectrometers, Detect. Assoc. Equip, vol. 569, no. 2, pp. 581–586, Dec. 2006, doi: 10.1016/J.NIMA.2006.08.137.

[16]. Van Leeuwen GMJJ, Hand JW, Lagendijk JJWW, Azzopardi DV, and Edwards AD, “Numerical modeling of temperature distributions within the neonatal head,” Pediatr. Res, vol. 48, no. 3, pp. 351–356, 2000. [PubMed: 10960502]

[17]. Sugiura T, Hirata H, Hand JW, Van Leeuwen JMJ, and Mizushina S, “Five-band microwave radiometer system for noninvasive brain temperature measurement in newborn babies: Phantom experiment and confidence interval,” Radio Sci, vol. 46, no. 5, pp. 1–7, Oct. 2011, doi: 10.1029/2011RS004736.

[18]. Rodrigues DB et al. , “Design and optimization of an ultra wideband and compact microwave antenna for radiometric monitoring of brain temperature,” IEEE Trans. Biomed. Eng, vol. 61, no. 7, pp. 2154–2160, Jul. 2014, doi: 10.1109/TBME.2014.2317484. [PubMed: 24759979]

[19]. Koutsoupidou M, Groumpas E, Karanasiou IS, Christopoulou M, Nikita K, and Uzunoglu N, “The effect of using a dielectric matching medium in focused microwave radiometry: An anatomically detailed head model study,” Med. Biol. Eng. Comput, vol. 56, no. 5, pp. 809–816, May 2018, doi: 10.1007/s11517-017-1729-4. [PubMed: 29027087]

[20]. “CST studio suite 3D EM simulation and analysis software,” Dassault Systemes. Accessed Sep. 16, 2020. [Online]. Available: https://www.3ds.com/products-services/simulia/products/cst-studio-suite

[21]. Stauffer PR et al. , “Non-invasive measurement of brain temperature with microwave radiometry: Demonstration in a head phantom and clinical case,” Neuroradiol. J, vol. 27, no. 1, pp. 3–12, 2014, doi: 10.15274/NRJ-2014-10001. [PubMed: 24571829]

[22]. Psikuta A, Niedermann R, and Rossi RM, “Effect of ambient temperature and attachment method on surface temperature measurements,” Int. J. Biometeorol, vol. 58, no. 5, pp. 877–885, May 2013, doi: 10.1007/S00484-013-0669-4. [PubMed: 23686110]

[23]. Gabriel C and Peyman A, “Dielectric measurement: Error analysis and assessment of uncertainty,” Phys. Med. Biol, vol. 51, no. 23, pp. 6033–6046, Dec. 2006, doi: 10.1088/0031-9155/51/23/006. [PubMed: 17110768]

[24]. Peyman A, Holden SJ, Watts S, Perrott R, and Gabriel C, “Dielectric properties of porcine cerebrospinal tissues at microwave frequencies: *In vivo, in vitro* and systematic

variation with age," Phys. Med. Biol, vol. 52, no. 8, pp. 2229–2245, Apr. 2007, doi: 10.1088/0031-9155/52/8/013. [PubMed: 17404466]

[25]. Bao JZ, Lu ST, and Hurt WD, "Complex dielectric measurements and analysis of brain tissues in the radio and microwave frequencies," IEEE Trans. Microw. Theory Techn, vol. 45, no. 10, pp. 1730–1741, Oct. 1997, doi: 10.1109/22.641720.

[26]. Kiourti A and Nikita KS, "Numerical assessment of the performance of a scalp-implantable antenna: Effects of head anatomy and dielectric parameters," Bioelectromagnetics, vol. 34, no. 3, pp. 167–179, Apr. 2013, doi: 10.1002/bem.21753. [PubMed: 22948753]

[27]. Tan S et al. , "Physical models of layered polar firn brightness temperatures from 0.5 to 2 GHz," IEEE J. Sel. Top. Appl. Earth Observ. Remote Sens, vol. 8, no. 7, pp. 3681–3691, Jul. 2015, doi: 10.1109/JSTARS.2015.2403286.

[28]. Tsang L, Kong JA, and Ding K-H, Scattering of Electromagnetic Waves: Theories and Applications. New York, NY, USA: Wiley, 2000.

[29]. Pennes HH, "Analysis of tissue and arterial blood temperatures in the resting human forearm," J. Appl. Physiol, vol. 1, no. 2, pp. 93–122, Aug. 1948, doi: 10.1152/jappl.1948.1.2.93. [PubMed: 18887578]

[30]. Rodrigues DB, Pereira PJS, Limão-Vieira P, Stauffer PR, and Maccarini PF, "Study of the one dimensional and transient bioheat transfer equation: Multi-layer solution development and applications," Int. J. Heat Mass Transf, vol. 62, no. 1, pp. 153–162, 2013, doi: 10.1016/j.ijheatmasstransfer.2012.11.082. [PubMed: 24511152]

[31]. Robinson JL, Seal RF, Spady DW, and Joffres MR, "Comparison of esophageal, rectal, axillary, bladder, tympanic, and pulmonary artery temperatures in children," J. Pediatr, vol. 133, no. 4, pp. 553–556, Oct. 1998, doi: 10.1016/S0022-3476(98)70067-8. [PubMed: 9787697]

[32]. Germann AM and Kashyap V, Anatomy, Head and Neck,Occipital Bone, Artery, Vein, and Nerve. Treasure Island, FL, USA: StatPearls Publishing, 2019.

[33]. Janssen FEM, Van Leeuwen GMJ, and Van Steen-hoven AA, "Modelling of temperature and perfusion during scalp cooling," Phys. Med. Biol, vol. 50, no. 17, pp. 4065–4073, Sep. 2005, doi: 10.1088/0031-9155/50/17/010. [PubMed: 16177530]

[34]. Gordon RG, Roemer RB, and Horvath SM, "A mathematical model of the human temperature regulatory system–transient cold exposure response," IEEE Trans. Biomed. Eng, vol. BME-23, no. 6, pp. 434–444, Nov. 1976, doi: 10.1109/TBME.1976.324601.

[35]. Zhu L and Diao C, "Theoretical simulation of temperature distribution in the brain during mild hypothermia treatment for brain injury," Med. Biol. Eng. Comput, vol. 39, no. 6, pp. 681–687, 2001, doi: 10.1007/BF02345442. [PubMed: 11804176]

[36]. Werner J and Buse M, "Temperature profiles with respect to inhomogeneity and geometry of the human body," J. Appl. Physiol, vol. 65, no. 3, pp. 1110–1118, 1988, doi: 10.1152/jappl.1988.65.3.1110. [PubMed: 3182480]

[37]. Steck LN, Sparrow EM, and Abraham JP, "Non-invasive measurement of the human core temperature," Int. J. Heat Mass Transf, vol. 54, no. 4, pp. 975–982, Jan. 2011, doi: 10.1016/j.ijheatmasstransfer.2010.09.042.

[38]. Neimark MA, Konstas AA, Choi JH, Laine AF, and Pile-Spellman J, "Brain cooling maintenance with cooling cap following induction with intracarotid cold saline infusion: A quantitative model," J. Theor. Biol, vol. 253, no. 2, pp. 333–344, Jul. 2008, doi: 10.1016/j.jtbi.2008.03.025. [PubMed: 18479713]

[39]. Blowers S et al. , "How does blood regulate cerebral temperatures during hypothermia?," Sci. Rep, vol. 8, no. 1, pp. 1–10, Dec. 2018, doi: 10.1038/s41598-018-26063-7. [PubMed: 29311619]

[40]. Chopra K et al. , "A comprehensive examination of topographic thickness of skin in the human face," Aesthetic Surg. J, vol. 35, no. 8, pp. 1007–1013, 2015, doi: 10.1093/asj/sjv079.

[41]. Kim Y et al. , "Regional thickness of facial skin and superficial fat: Application to the minimally invasive procedures," Clin. Anatomy, vol. 32, no. 8, pp. 1008–1018, Nov. 2019, doi: 10.1002/ca.23331.

[42]. Wendel-Mitoraj K, Malmivuo J, and Hyttinen JA, "Measuring tissue thicknesses of the human head using centralized and normalized trajectories," in Proc. Conf. Consciousness Measures, St. Raphael Hotel, Limassol, Cyprus, Nov. 2009, pp. 112–113, Accessed: Sep. 16, 2020. [Online].

Available: https://www.researchgate.net/publication/283625027_Measuring_Tissue_Thicknesses_of_the_Human_Head_Using_Centralized_and_Normalized_Trajectories

[43]. Frank K et al. , "Age and gender differences of the frontal bone: A computed tomographic (CT)-Based study," Aesthetic Surg. J, vol. 39, no. 7, pp. 699–710, Jun. 2019, doi: 10.1093/asj/sjy270.

[44]. Haeussinger FB, Heinzel S, Hahn T, Schecklmann M, Ehlis AC, and Fallgatter AJ, "Simulation of near-infrared light absorption considering individual head and prefrontal cortex anatomy: Implications for optical neuroimaging," PLoS One, vol. 6, no. 10, Oct. 2011, Art. no. 26377, doi: 10.1371/journal.pone.0026377.

[45]. Ramon C, Garguilo P, Fridgeirsson EA, and Haueisen J, "Changes in scalp potentials and spatial smoothing effects of inclusion of dura layer in human head models for EEG simulations," Front. Neuroeng, vol. 7, Aug. 2014, Art. no. 32, doi: 10.3389/fneng.2014.00032. [PubMed: 25140148]

[46]. Alexander SL, Rafaels K, Gunnarsson CA, and Weerasooriya T, "Structural analysis of the frontal and parietal bones of the human skull," J. Mech. Behav. Biomed. Mater, vol. 90, pp. 689–701, Feb. 2019, doi: 10.1016/j.jmbbm.2018.10.035. [PubMed: 30530225]

[47]. Volk GF, Leier C, and Guntinas-lichius O, "Correlation between electromyography and quantitative ultrasonography of facial muscles in patients with facial palsy," Muscle Nerve, vol. 53, no. 5, pp. 755–761, May 2016, doi: 10.1002/mus.24931. [PubMed: 26439679]

[48]. Ogoina D, "Fever, fever patterns and diseases called 'fever' - A review," J. Infection Public Health, vol. 4, no. 3, pp. 108–124, Aug. 2011, doi: 10.1016/j.jiph.2011.05.002. [PubMed: 21843857]

[49]. Andreuccetti D, Fossi R, and Petrucci C, "Dielectric properties of body tissues," Italian Nat. Res. Council Inst. Appl. Phys, 2015, Accessed: Sep. 16, 2020. [Online]. Available: http://niremf.ifac.cnr.it/tissprop/htmlclie/htmlclie.php

[50]. Gabriel S, Lau RW, and Gabriel C, "The dielectric properties of biological tissues: III. Parametric models for the dielectric spectrum of tissues," Phys. Med. Biol, vol. 41, no. 11, pp. 2271–2293, Nov. 1996, doi: 10.1088/0031-9155/41/11/003. [PubMed: 8938026]

[51]. Gabriel C, Gabriel S, and Corthout E, "The dielectric properties of biological tissues: I. Literature survey," Phys. Med. Biol, vol. 41, no. 11, pp. 2231–2249, Nov. 1996, doi: 10.1088/0031-9155/41/11/001. [PubMed: 8938024]

[52]. Gabriel S, Lau RW, and Gabriel C, "The dielectric properties of biological tissues: II. Measurements in the frequency range 10 Hz to 20 GHz," Phys. Med. Biol, vol. 41, no. 11, pp. 2251–2269, Nov. 1996, doi: 10.1088/0031-9155/41/11/002. [PubMed: 8938025]

[53]. Xu L, Meng MQH, and Chan Y, "Effects of dielectric parameters of human body on radiation characteristics of ingestible wireless device at operating frequency of 430 MHz," IEEE Trans. Biomed. Eng, vol. 56, no. 8, pp. 2083–2094, Aug. 2009, doi: 10.1109/TBME.2009.2021157. [PubMed: 19605308]

[54]. Keshvari J, Keshvari R, and Lang S, "The effect of increase in dielectric values on specific absorption rate (SAR) in eye and head tissues following 900, 1800 and 2450 MHz radio frequency (RF) exposure," Phys. Med. Biol, vol. 51, no. 6, pp. 1463–1477, Mar. 2006, doi: 10.1088/0031-9155/51/6/007. [PubMed: 16510956]

[55]. Blauert J and Kiourti A, "Theoretical modeling and design guidelines for a new class of wearable bio-matched antennas," IEEE Trans. Antennas Propag, vol. 68, no. 8, pp. 2040–2049, Aug. 2020, doi: 10.1109/TAP.2018.2889159.

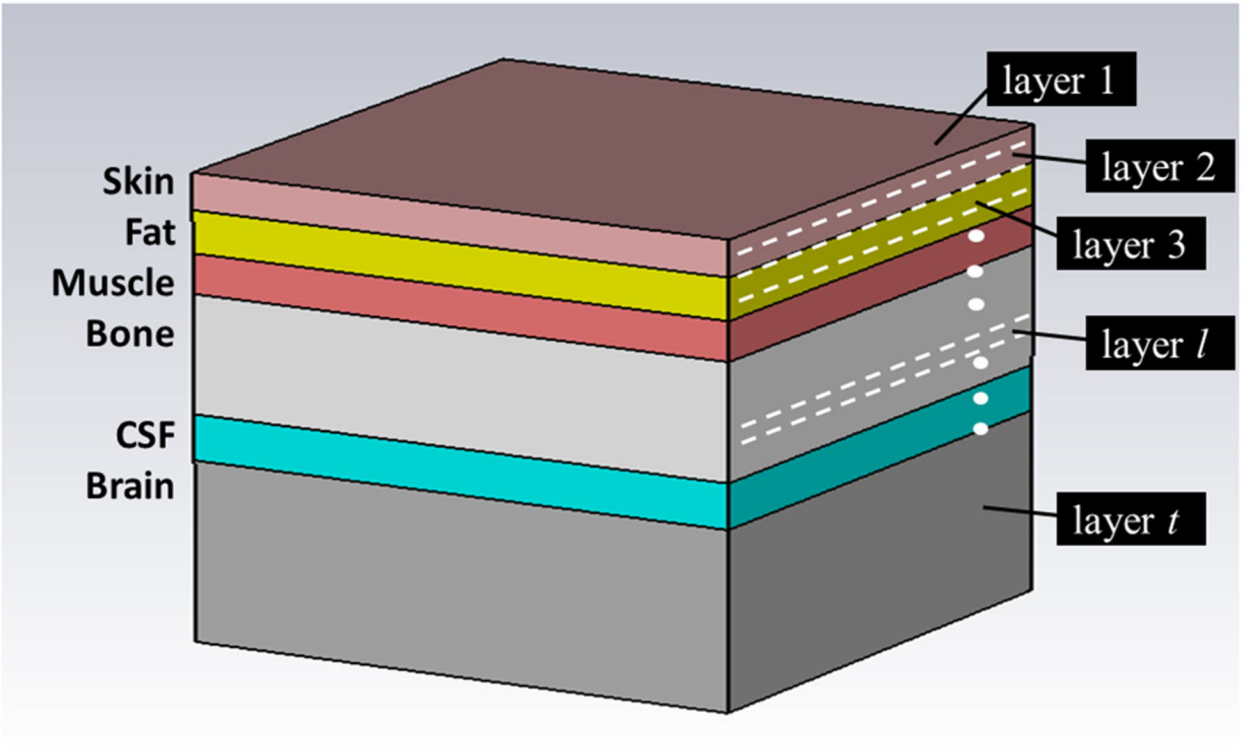

Fig. 1.

The six-layer model of the human head used for this analysis. Tissue layers are denoted on the left, while layers for the coherent model are denoted on the right.

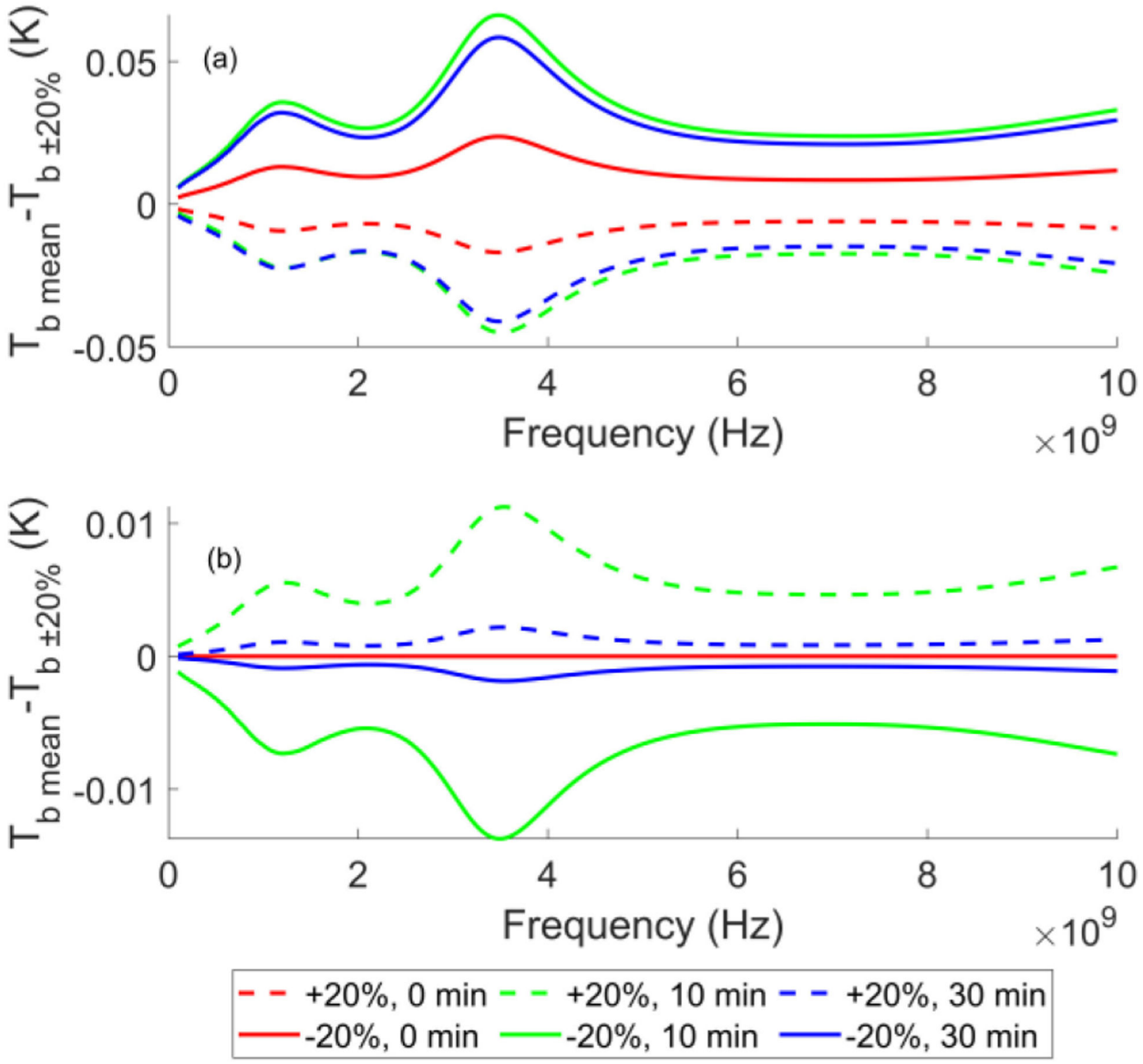

Fig. 2.

Difference between the mean brightness temperature profile and that of ±20% of the (a) CSF thermal conductivity and (b) muscle specific heat at 0, 10, and 30 min into the experiment. Varying thermal conductivity affects both the steady state and transient profiles, whereas specific heat affects only the transient profile.

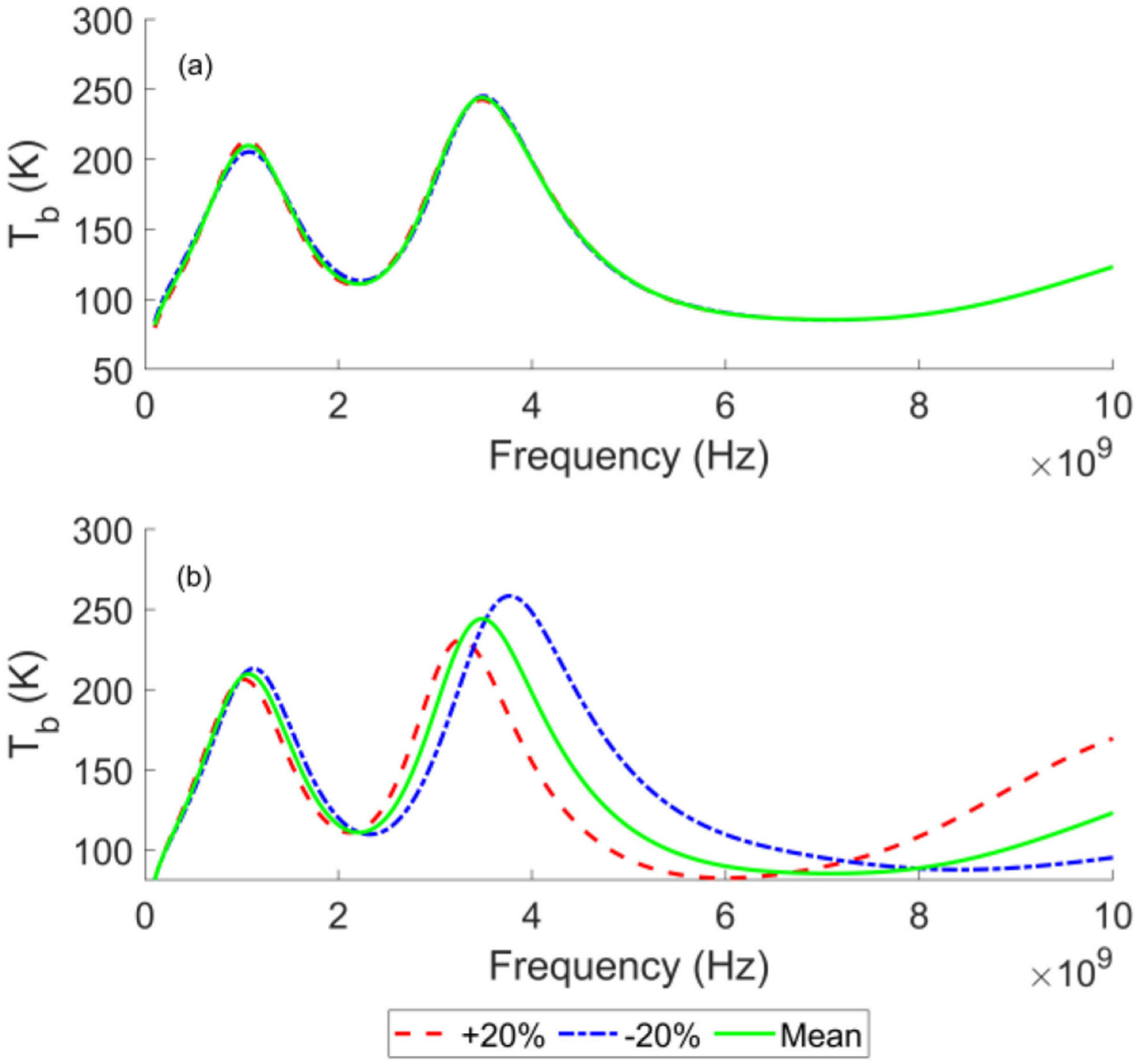

Fig. 3.

Brightness temperature at 0 min (normothermic, steady state core) when (a) CSF and (b) skin thickness is varied by ±20%. A smaller shift in the maxima frequency occurs since CSF and brain have a similar permittivity, whereas varying skin thickness has a large effect on the frequency at which the second maximum occurs.

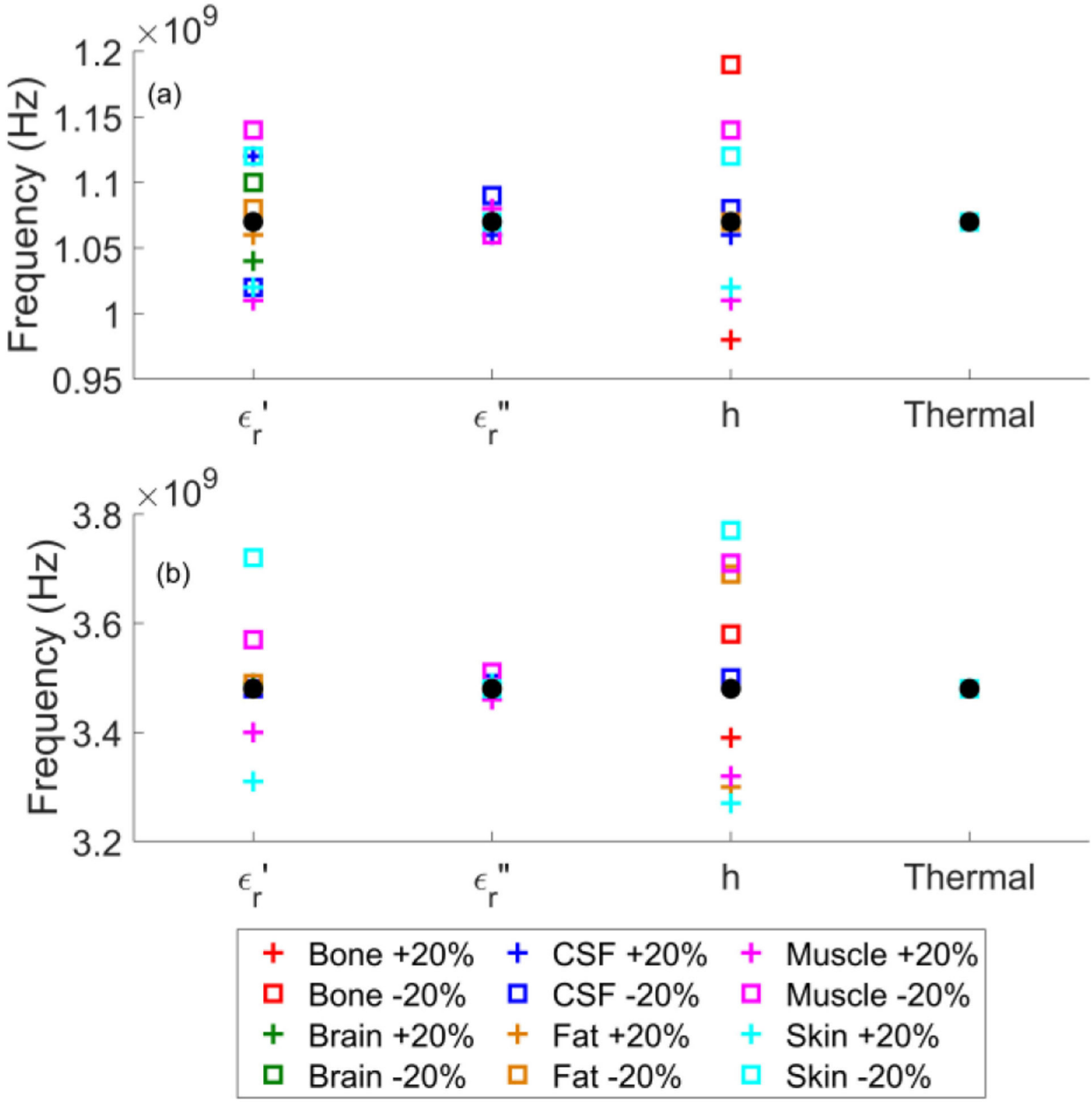

Fig. 4.

Frequency of occurrence for the (a) low frequency and (b) high frequency maxima when the EM and thermal parameters are varied by ±20% in each layer. Varying the thermal parameters does not change the maxima frequencies, so they are grouped together. Real permittivity and tissue layer thickness have the greatest effect on the brightness temperature maxima frequency.

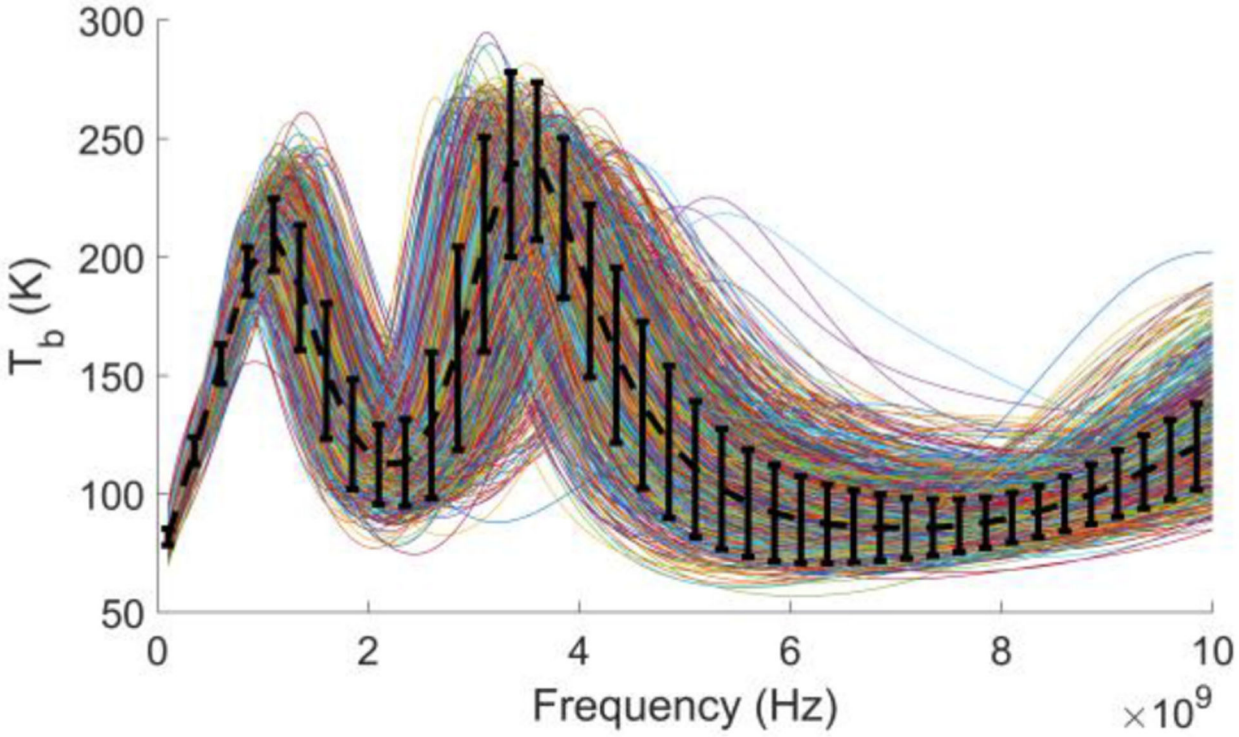

Fig. 5.

All 1000 brightness temperature profiles compared to the mean profile (black dashed line) at 0 min. The black bars represent the standard deviation in brightness temperature. A single core physical temperature can result in many different brightness temperatures given parameter variation within the human population.

TABLE I

Thermal and EM Parameter Distributions

	Mean	Std Dev	Std Dev %
h [mm] brain	30.000	-	-
CSF	3.600	0.900	25%
bone	6.576	0.752	11%
muscle	2.210	0.640	29%
fat	2.353	0.561	24%
skin	2.044	0.171	8%
k [W/(m·K)] brain	0.516	0.019	4%
CSF	0.533	0.058	11%
bone	0.931	0.295	32%
muscle	0.487	0.059	12%
fat	0.191	0.025	13%
skin	0.319	0.102	32%
c [kJ/(K·kg)] brain	3.710	0.066	2%
CSF	3.872	0.215	6%
bone	1.739	0.340	20%
muscle	3.705	0.138	3%
fat	2.430	0.090	4%
skin	3.675	0.109	3%
p [kg/m^3] brain	1032.0	23.6	2%
CSF	1000.0	0	0%
bone	1545.0	174.4	11%
muscle	1059.0	23.2	2%
fat	911.3	74.0	8%
skin	1051.0	47.8	5%
Q_m [W/m^3] brain	8202.0	2586.0	32%
CSF	0	0	0%
bone	416.6	108.1	26%
muscle	623.3	124.6	20%
fat	322.7	39.26	12%
skin	1375.0	394.0	29%
B [W/(m^3 .K)] brain	31297	8377	27%
CSF	0	0	0%
bone	1416	273	19%
muscle	2303	349	15%
fat	478	159	33%
skin	9817	3272	33%
ε', ε" (all layers)	Frequency-dependent, from [49]	-	10%

TABLE II

Maximum Difference in Average Layer Temperature (°C) and Layer of Occurrence for ±20% Thermal Parameter Change

Layer of Parameter Change	h		k		B		c		ρ		Q	
	Max Δ°C	Layer	Max Δ°C	Layer	Max Δ°C	Layer	Max Δ°C	Layer	Max Δ°C	Layer	Max Δ°C	Layer
CSF	0.1966	Bone	0.1573	Bone	-	-	0.0457	CSF	0.0648	CSF	-	-
Bone	0.1291	Fat	0.1034	Fat	0.0327	CSF	0.0652	Bone	0.0566	Bone	0.0267	CSF
Muscle	0.0723	Fat	0.0619	Fat	0.0283	CSF	0.0302	Muscle	0.0297	Muscle	0.0435	CSF
Fat	0.1065	Skin	0.1181	Skin	0.0154	CSF	0.0209	Fat	0.0186	Fat	0.0293	Muscle
Skin	0.1108	Fat	0.0319	Fat	0.1071	Skin	0.0251	Skin	0.0455	CSF	0.0558	CSF